Multifidelity Uncertainty Propagation via Adaptive Surrogates in Coupled Multidisciplinary Systems

Anirban Chaudhuri*, Remi Lam† and Karen Willcox‡
Massachusetts Institute of Technology, Cambridge, MA, 02139, USA

Fixed point iteration is a common strategy to handle interdisciplinary coupling within a feedback-coupled multidisciplinary analysis. For each coupled analysis, this requires a large number of disciplinary high-fidelity simulations to resolve the interactions between different disciplines. When embedded within an uncertainty analysis loop (e.g., with Monte Carlo sampling over uncertain parameters) the number of high-fidelity disciplinary simulations quickly becomes prohibitive, since each sample requires a fixed point iteration and the uncertainty analysis typically involves thousands or even millions of samples. This paper develops a method for uncertainty quantification in feedback-coupled systems that leverages adaptive surrogates to reduce the number of cases for which fixed point iteration is needed. The multifidelity coupled uncertainty propagation method is an iterative process that uses surrogates for approximating the coupling variables and adaptive sampling strategies to refine the surrogates. The adaptive sampling strategies explored in this work are residual error, information gain, and weighted information gain. The surrogate models are adapted in a way that does not compromise accuracy of the uncertainty analysis relative to the original coupled high-fidelity problem as shown through a rigorous convergence analysis.

I. Introduction

This work proposes a new multifidelity uncertainty propagation method for feedback-coupled multidisciplinary systems. Multidisciplinary analysis and optimization is an extensive area of research focused on methods that take into account the interactions between multiple disciplines, working towards building an efficient engineering system.[1,2,3,4] Optimization of such complex systems often pushes the designs close to failure limits, which makes accounting for inherent system uncertainties paramount. Historically, uncertainties are accounted for by using safety factors; however, the drive to enhance system efficiency and robustness requires more rigorous uncertainty characterization methods. To be practically applicable, these methods must also be computationally efficient. The new method proposed in this paper balances these dual goals of computational efficiency and rigor.

A review of existing methods in uncertainty analysis for multidisciplinary optimization can be found in Yao et al.[5] The task of uncertainty analysis—forward propagation of uncertainty from inputs to outputs through a system—is particularly challenging for a multidisciplinary system due to coupling between different disciplines. This coupling could be feed-forward (one-directional) or feedback (bidirectional). Feed-forward coupling is usually easier to deal with; it has been tackled using approximations such as surrogates[6] and decomposition combined with recomposition through importance sampling.[7] Here, we focus on the more challenging case of uncertainty analysis of feedback-coupled systems. Such systems arise in many aerospace engineering applications, such as aero-structural-thermal coupling in hypersonic flights,[8] turbine engine cycle analysis,[9] satellite performance analysis,[10,11] topology optimization,[12] and many more. Our approach is non-intrusive (i.e., it treats all disciplinary analyses as black-boxes that are viewed in terms of their inputs and outputs without requiring knowledge of the internal model mechanisms) and thus it is broadly applicable to this class of problems.

One of the major challenges in feedback-coupled systems is to obtain multidisciplinary feasible solutions.[13] A common method to do this is through fixed point iteration (FPI).[13,14,15] In FPI, the outputs from one

*Postdoctoral Associate, Department of Aeronautics and Astronautics, anirbanc@mit.edu, AIAA member.
†Graduate Research Assistant, Department of Aeronautics and Astronautics, rlam@mit.edu, AIAA student member.
‡Professor, Department of Aeronautics and Astronautics, kwillcox@mit.edu, AIAA Associate Fellow.

discipline are fed as inputs to the coupled discipline and this process iterates until a multidisciplinary feasible solution is reached. Each iteration within the FPI requires disciplinary high-fidelity solves, thus the method becomes computationally intensive as the number of iterations for FPI convergence increases. When FPI is embedded within Monte Carlo simulation for uncertainty propagation, the number of high-fidelity simulations can quickly become computationally prohibitive.

Past work has tackled uncertainty analysis of feedback-coupled systems by approximating the coupling variables and outputs using surrogates. The surrogate models are then used in place of the high-fidelity FPI simulations to propagate the uncertainty. In particular, stochastic expansion methods using polynomial chaos expansions combined with dimension reduction have been explored for feedback-coupled systems.[16,17] Hybrid methods that combine Monte Carlo sampling and stochastic expansion methods for stochastic coupled problems have also been studied.[18,19] Another approach uses Gaussian Process surrogates to estimate low-order statistical moments of system outputs in the presence of epistemic and aleatory uncertainties.[20] These methods are efficient if the surrogate predictions of the coupling variables and outputs are accurate; however, these existing methods all typically lack guarantees of convergence to the fixed point solutions of the original high-fidelity system.

Decoupling is another approach for dealing with uncertainty analysis of feedback-coupled systems. These methods include fully decoupled approaches such as collaborative reliability analysis[21] and the first order reliability method (FORM),[22] and partially decoupled approaches such as the likelihood-based approach that approximates a feedback-coupled system as a feed-forward system.[23] Decoupling approaches are efficient because they avoid feedback-coupled system analyses and the associated FPI, but at the cost of neglecting the dependence between the inputs and the coupling variables. This can be effective if the goal is to estimate the statistics of the coupling variables or when the sensitivity of the system output to coupling variables is low. However, it can lead to poor results when sensitivity of the system outputs to the coupling variables is high. In these cases, even if each discipline model itself is accurate, an improper representation of the interdependent effects of disciplinary coupling leads to inaccurate estimation of the system output distribution.

In this work, we introduce an approach that maintains the accuracy of the mapping from the inputs to the system outputs and uses adaptive surrogates for the coupling variables to reduce the number of cases for which FPI is executed in the Monte Carlo simulation of a feedback-coupled system. The surrogates are constructed in terms of the input random variables using multidisciplinary feasible solutions of the coupling variables and are iteratively refined using adaptive sampling based on an information-gain metric and a residual-error metric. Various adaptive sampling strategies have been previously explored for surrogate-based optimization.[24,25] Adaptive sampling for estimating reliability by refining around the limit state boundary has been investigated based on expected feasibility functions.[26,27] Information-gain-based approaches have been used previously for global optimization[28,29,30] and optimal experimental design.[31,32] Our work differs from previous efforts in that we develop adaptive sampling strategies in the context of uncertainty propagation in coupled multidisciplinary systems—our adaptation approach exploits the particular structure of the feedback-coupled analysis. Our proposed method increases the computational efficiency for uncertainty propagation, while not compromising the accuracy relative to the results obtained by using Monte Carlo simulation with FPI, as we show through a rigorous convergence analysis.

The remainder of the paper is organized as follows. Section II presents the problem statement for uncertainty analysis of a feedback-coupled system. Section III provides the details of the multifidelity coupled uncertainty propagation method and its convergence analysis. Section IV presents numerical experiments that compare the efficiency of the proposed method to that of the standard FPI approach. Section V provides the conclusions.

II. Multidisciplinary Coupled Uncertainty Propagation: Problem Setup

A generic feedback-coupled multidisciplinary system is shown in Figure 1. For the example depicted, the number of disciplines $N_D = 3$, with discipline 1 and discipline 2 being feedback-coupled through coupling variables C_1 and C_2. Here, the number of coupling variables is $N_C = 2$. The coupling variable C_1 is an input for discipline 2 and an output for discipline 1. The coupling variable C_2 is an input for discipline 1 and an output for discipline 2. Let C_1^* and C_2^* be the multidisciplinary feasible solution of the coupling variables for the feedback-coupled system, which is achieved when the interdisciplinary coupling constraints are satisfied (see Cramer et al.[13] for a detailed discussion on problem formulation for multidisciplinary systems).

The variables $y^{(1)}$ and $y^{(2)}$ represent the disciplinary outputs from discipline 1 and 2, respectively, and S is the system output computed by discipline 3. The multidisciplinary system is described by the set of high-fidelity models $\mathbf{H} = \{H_{C_1}(C_2, \mathbf{x}), H_{C_2}(C_1, \mathbf{x}), H_{y^{(1)}}(C_1^*, C_2^*, \mathbf{x}), H_{y^{(2)}}(C_1^*, C_2^*, \mathbf{x}), H_S(\mathbf{y}, C_1^*, C_2^*, \mathbf{x})\}$ with input vector $\mathbf{x} \in \mathbb{R}^{dim}$ and disciplinary output vector $\mathbf{y} = [y^{(1)}, y^{(2)}]^T$. The inputs could be independent or shared inputs for different disciplines. Note that in this description we treat the coupling variables and outputs of each discipline as scalars but in general they could be multidimensional vectors. All theories developed in this work can be extended to such cases. Also note that while Figure 1 shows only two feedback-coupled disciplines, our approach extends to the case of multiple feedback-coupled disciplines.

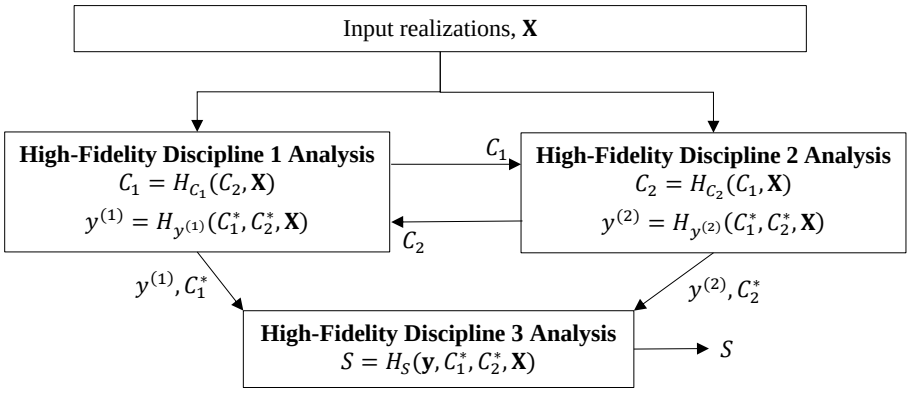

Figure 1. Feedback coupled multidisciplinary system

The aim of this work is to quantify uncertainty in disciplinary outputs $\mathbf{y}$ and system output S due to uncertainty in inputs $\mathbf{x}$. We consider uncertainty in the inputs defined by a probability distribution function, $\pi_{\mathbf{x}}$. To estimate the corresponding uncertainty in $\mathbf{y}$ and S, we use Monte Carlo simulation. Consider N_{total} input realizations $\mathbf{x}_1, \ldots, \mathbf{x}_{N_{total}}$ drawn randomly from $\pi_{\mathbf{x}}$. The Monte Carlo simulation propagates each of these samples through the system analysis and generates the corresponding output sample $\mathbf{y}_1, \ldots, \mathbf{y}_{N_{total}}$. Let $\mathbf{X} = \{\mathbf{x}_1, \ldots, \mathbf{x}_{N_{total}}\}$ be the set of N_{total} input realizations. For each input realization, we must solve the feedback-coupled multidisciplinary system. As noted before, FPI is a common method to do this. For the depicted example, at a given realization $\mathbf{x}_i$, the FPI is initialized with an arbitrary value of one of the coupling variables. For example, an initial guess for C_1 is used for discipline 2 to calculate the value of C_2 and feed that value of C_2 to discipline 1 to calculate C_1. The output C_1 from discipline 1 is again fed into discipline 2 and the process iterates until the multidisciplinary feasible solution is reached. A multidisciplinary feasible solution obtained using FPI is denoted by $[C_1^{FPI}, C_2^{FPI}]^T$. Note that here we assume $\forall\ \mathbf{x}_i \in \mathbf{X}\ \exists\ [C_1^{FPI}, C_2^{FPI}]^T$, i.e., for each input realization in $\mathbf{X}$ there exists at least one fixed point solution for the feedback-coupled system.

III. Multifidelity Coupled Uncertainty Propagation via Adaptive Surrogates

We propose a multifidelity coupled uncertainty propagation method that reduces the number of cases for which we need to perform FPI and thus reduces the number of required high-fidelity disciplinary simulations. This section gives an overview of the approach, describes the adaptive sampling strategies, and discusses convergence.

A. Approach Overview

Figure 2 presents a flowchart detailing the multifidelity coupled uncertainty propagation method and the blocks described by Algorithms 1 and 2. This flowchart uses the same definitions from the example described in Figure 1. Note that the approach applies to multiple disciplines and multi-dimensional coupling variables, but the simpler case is shown for ease of exposition. The method is an iterative process that uses surrogate models for approximating the coupling variables, with the approximate coupling variables denoted by $\widetilde{C}$. Here, we use a Kriging surrogate,[33,34] but one could use any surrogate that is equipped with an uncertainty estimate.

Given the set $\mathbf{X}$ of N_{total} input realizations, we first select a subset of N_{sur} initial samples, $\mathbf{X}^0_{sur} \subset \mathbf{X}$. The superscript 0 represents the 0^{th} cycle of the method to denote initial samples for training the surrogates. The subset selection can be conducted in any way, but here we maximize the minimum distance between the samples in order to obtain coverage across the input space. Then FPI is conducted for the coupled system at each of the N_{sur} samples to obtain the multidisciplinary feasible solutions of the coupling variables at those samples. We denote the resulting vector of multidisciplinary feasible solutions of the i^{th} coupling variable as $C_i^{FPI}(\mathbf{X}^0_{sur})$. The dataset $\{\mathbf{X}^0_{sur}; C_i^{FPI}(\mathbf{X}^0_{sur})\}$ is used to build the surrogate for the i^{th} coupling variable. Since FPI is performed for all the realizations in $\mathbf{X}^0_{sur}$, the multidisciplinary feasible coupled system output can be calculated for these cases. The system outputs for the realizations obtained through FPI and those satisfying the residual error tolerance (discussed later in this section) are included in the set of accepted system outputs, $\mathbf{S}_{accept}$. The accepted system outputs after the 0^{th} cycle are given by $\mathbf{S}_{accept} = \{S(\mathbf{X}^0_{sur})\}$. The set of remaining input realizations is given by $\mathbf{X}^0_{rem} = \mathbf{X} \setminus \mathbf{X}^0_{sur}$ and the number of remaining samples is given by $N^0_{rem} = N_{total} - N_{sur}$. These initialization steps are shown in Algorithm 1.

Algorithm 1 Initialization for the uncertainty propagation method

procedure INITIALIZATION($N_D, N_C, N_{sur}, \mathbf{X}$)
  Select N_{sur} initial samples for building surrogate, $\mathbf{X}^0_{sur} \subset \mathbf{X}$, by maximizing the minimum distance between the samples
  Perform FPI to get multidisciplinary feasible solution for the N_C coupling variables at the selected $\mathbf{X}^0_{sur}$ locations, $C_i^{FPI}(\mathbf{X}^0_{sur}), \forall i = 1, \ldots, N_C$
  Build N_C surrogates for coupling variables using the dataset $\{\mathbf{X}^0_{sur}; C_i^{FPI}(\mathbf{X}^0_{sur})\}, \forall i = 1, \ldots, N_C$
  $\mathbf{S}_{accept} \leftarrow \{S(\mathbf{X}^0_{sur})\}$ ▷ Set of accepted system outputs for indicated realizations
  $\mathbf{X}^0_{rem} \leftarrow \mathbf{X} \setminus \mathbf{X}^0_{sur}$ ▷ Remaining realizations
  $N^0_{rem} \leftarrow N_{total} - N_{sur}$ ▷ Number of remaining realizations
  return $\mathbf{X}^0_{rem}, N^0_{rem}, \mathbf{X}^0_{sur}, \mathbf{S}_{accept}$
end procedure

Then the set of remaining input realizations, $\mathbf{X}^0_{rem}$, and the surrogate predictions for the coupling variables are propagated through the respective high-fidelity disciplinary analysis to estimate the outputs. Note that FPI is not performed at this point and the high-fidelity simulations of the coupled disciplines can be decoupled as seen in Figure 2. A normalized residual error metric e^t at the current cycle t for the approximation of the coupling variables is defined as

$$e^t(\mathbf{x}) = \sum_{i=1}^{N_C} \frac{\left|\widetilde{C}_i^t(\mathbf{x}) - C_i^{out}(\mathbf{x})\right|}{\kappa_i}, \tag{1}$$

where $\widetilde{C}_i^t$ is the surrogate model prediction at the current cycle t, C_i^{out} is the output from the high-fidelity analysis of the i^{th} coupling variable, κ_i is the normalization constant for the residual errors of the i^{th} coupling variable, and N_C is the number of coupling variables. The normalization constants are problem specific and will be specified with the respective test problems. The system outputs for the realizations $\mathbf{x}$ that satisfy the residual error tolerance criterion $e^t(\mathbf{x}) \leq \varepsilon$, where ε is a user-defined residual error tolerance, are accepted ($\mathbf{S}_{accept} = \mathbf{S}_{accept} \cup \{S(\mathbf{x}), \forall \mathbf{x} \in \mathbf{X}^t_{rem} : e^t(\mathbf{x}) \leq \varepsilon\}$).

Let $\mathbf{X}^t_{rem} = \{\mathbf{x} \in \mathbf{X} \setminus \mathbf{X}^t_{sur} : e^t(\mathbf{x}) > \varepsilon\}$ be the set of N^t_{rem} realizations that did not satisfy the error tolerance. An adaptive sampling strategy (described in detail in Section III. B) is used to select one of these realizations, $\mathbf{x}^*_t \in \mathbf{X}^t_{rem}$. For the selected realization, FPI is used to solve for the multidisciplinary feasible solution, $C_i^{FPI}(\mathbf{x}^*_t)$, for $i = 1, \ldots, N_C$.

The surrogate model for the i^{th} coupling variable is then refined using $\mathbf{X}^{t+1}_{sur} = \mathbf{X}^t_{sur} \cup \{\mathbf{x}^*_t\}$ and the updated dataset $\{\mathbf{X}^{t+1}_{sur}; C_i^{FPI}(\mathbf{X}^{t+1}_{sur})\}$. No additional high-fidelity simulations are required during the selection of $\mathbf{x}^*_t$ with the adaptive sampling strategy. In the next cycle, $\mathbf{X}^t_{rem}$ realizations are propagated through the layers of surrogates and high-fidelity models as described above to find the realizations for which the error in Equation 1 is not acceptable, $\mathbf{X}^{t+1}_{rem}$. This proceeds iteratively till $\mathbf{X}^{t+1}_{rem} = \emptyset$. The uncertainty propagation procedure is described in Algorithm 2.

Note that the proposed method works by building surrogates for the coupling variables as a function of the input random variables, rather than building surrogates for the disciplinary outputs or system outputs

Algorithm 2 Multifidelity coupled uncertainty propagation

procedure UNCERTAINTYPROPAGATION($N_D, N_C, N_{sur}, N^0_{rem}, \mathbf{X}^0_{rem}, \mathbf{X}^0_{sur}, \mathbf{S}_{accept}, \varepsilon$)
  $t \leftarrow 0$ ▷ Cycle number
  while $N^t_{rem} > 1$ **do**
    Evaluate surrogate predictions for coupling variables, $\widetilde{C}^t_i, \forall i = 1, \ldots, N_C$
    Propagate $\mathbf{X}^t_{rem}$ and $\widetilde{C}^t_i$ through all high-fidelity disciplinary analysis to estimate outputs $y^{(k)}, \forall k = 1, \ldots, N_D$ and $C^{out}_i, \forall i = 1, \ldots, N_C$ ▷ Decoupled analysis: no FPI performed
    Evaluate normalized residual error, $e^t(\mathbf{x})$ using Equation 1
    $\mathbf{S}_{accept} \leftarrow \mathbf{S}_{accept} \cup \{S(\mathbf{x}), \forall \mathbf{x} \in \mathbf{X}^t_{rem} : e^t(\mathbf{x}) \leq \varepsilon\}$
    $t \leftarrow t + 1$
    $\mathbf{X}^t_{rem} \leftarrow \{\mathbf{x} \in \mathbf{X}^{t-1}_{rem} : e^t(\mathbf{x}) > \varepsilon\}$
    $N^t_{rem} \leftarrow |\mathbf{X}^t_{rem}|$
    if $N^t_{rem} > 1$ **then** ▷ Perform adaptive sampling
      Find $\mathbf{x}^*_t$ for the selected adaptive sampling strategy using Equations 2, 10 or 12
      Perform FPI at $\mathbf{x}^*_t$ to get $C^{FPI}_i(\mathbf{x}^*_t), \forall i = 1, \ldots, N_C$
      $\mathbf{X}^t_{sur} \leftarrow \mathbf{X}^{t-1}_{sur} \cup \{\mathbf{x}^*_t\}$
      Updated surrogates using $\{\mathbf{X}^t_{sur}; C^{FPI}_i(\mathbf{X}^t_{sur})\}, \forall i = 1, \ldots, N_C$
      $N_{sur} \leftarrow N_{sur} + 1$
      $\mathbf{S}_{accept} \leftarrow \mathbf{S}_{accept} \cup \{S(\mathbf{x}^*_t)\}$
      $\mathbf{X}^t_{rem} \leftarrow \mathbf{X}^t_{rem} \setminus \{\mathbf{x}^*_t\}$
    end if
  end while
  if $N^t_{rem} == 0$ **then**
    return S_{accept}
  else ▷ $N^t_{rem} = 1$
    Perform FPI for the one remaining realization in $\mathbf{X}^t_{rem}$
    $\mathbf{S}_{accept} \leftarrow \mathbf{S}_{accept} \cup \{S(\mathbf{X}^t_{rem})\}$
    return $\mathbf{S}_{accept}$
  end if
end procedure

directly. The reasons that motivate this choice are two-fold. Firstly, building surrogates for the coupling variables permits us to exploit the properties of feedback-coupled analyses to design an adaptive sampling strategy for iteratively refining the surrogates by quantifying the residual error for the convergence of the coupling variables. Secondly, monitoring the residual error for the coupling variables in order to accept or reject a solution ensures convergence to the fixed point solutions based on the residual error tolerance. In contrast, if one were to build surrogates for the disciplinary outputs or the system outputs directly, it is not clear how to define adaptive sampling strategies or to prove convergence, because there is no obvious method to quantify the error in the solution.

The major advantage of this method is that it maintains a similar level of accuracy as the uncertainty analysis of high-fidelity coupled system using FPI for all the realizations in $\mathbf{X}$ (analyzed in more detail in Section III. C). The proposed method does not perform FPI for all $\mathbf{x} \in \mathbf{X}$. FPI is performed only for the initial $\mathbf{X}^0_{sur}$ realizations and the selected $\mathbf{x}^*_t$ realizations in each cycle through the adaptive sampling process. As the results will show, this can lead to substantial computational savings without compromising accuracy. Another advantage of the method is that, although the high-fidelity coupled disciplinary analyses for FPI cannot be decoupled, the remainder of the high-fidelity disciplinary analyses can be decoupled as shown in the flowchart (Figure 2). This would be favorable when communication between the disciplines is difficult due to their development by different working groups or the analyses running on separate platforms. Even though we partially decouple the process, we still recover the one-to-one mapping between the inputs and the system outputs through the iterative process.

B. Adaptive Sampling Strategies

Three different adaptive sampling strategies for selecting the $\mathbf{x}^*_t$ realization, which is used to update the surrogate models, are explored for the multifidelity coupled uncertainty propagation method.

1. Maximum Residual Error

In this sampling strategy, the realization $\mathbf{x}^*_t \in \mathbf{X}^t_{rem}$ with maximum normalized residual relative error is selected as the next sample. For cycle t, the optimization problem for the maximum residual error adaptive sampling strategy is given by

$$\mathbf{x}^*_t = \underset{\mathbf{x}\in\mathbf{X}^t_{rem}}{\operatorname{argmax}} \sum_{i=1}^{N_C} \frac{\left|\widetilde{C}^t_i(\mathbf{x}) - C^{out}_i(\mathbf{x})\right|}{\kappa_i}. \tag{2}$$

2. Maximum Information Gain

Using information gain as the sampling strategy enables us to use the surrogate prediction as well as the surrogate prediction standard deviation to make a decision on where to sample next. Note that both of these quantities are available from the Kriging fit that is used in this work. The Kriging surrogate prediction at any location in the design space, $\mathbf{x}$, is defined by a Gaussian distribution with mean prediction, $\mu(\mathbf{x})$, and prediction standard deviation, $\sigma(\mathbf{x})$. This adaptive sampling strategy chooses the next sampling location such that there will be maximum information gain in the surrogate prediction at the locations corresponding to the realizations in $\mathbf{X}^t_{rem}$.

In order to evaluate the information gain, a possible future surrogate is constructed by assuming a possible future data value at the potential sampling location. Then the change in the predicted Gaussian distributions from the present and future surrogates at the remaining locations is quantified by the Kullback-Leibler (KL) divergence, which represents the information gain. We denote the present surrogate predicted Gaussian distribution as $G_P(\mathbf{x}|d) \sim \mathcal{N}(\mu_P(\mathbf{x}|d), \sigma^2_P(\mathbf{x}|d))$ and a possible future surrogate predicted Gaussian distribution as $G_F(\mathbf{x}|d, \mathbf{x}_F, \widetilde{C}^F_i) \sim \mathcal{N}(\mu_F(\mathbf{x}|d, \mathbf{x}_F, \widetilde{C}^F_i), \sigma^2_F(\mathbf{x}|d, \mathbf{x}_F, \widetilde{C}^F_i))$. $\widetilde{C}^F_i$ is a possible future value at $\mathbf{x}_F$ defined here as a realization of the Gaussian distribution $G_P(\mathbf{x}_F|d)$. The KL divergence between G_P and G_F at any realization $\mathbf{x}$, given the data $d = \{\mathbf{X}^t_{sur}; C^{FPI}_i(\mathbf{X}^t_{sur})\}$ and possible future data value $\{\mathbf{x}_F; \widetilde{C}^F_i\}$ for the i^{th} coupling variable, is defined by

$$\begin{aligned} &D_{KL}(G_P(\mathbf{x}|d) \parallel G_F(\mathbf{x}|d, \mathbf{x}_F, \widetilde{C}^F_i)) \\ &\quad = log\left(\frac{\sigma_F(\mathbf{x}|d, \mathbf{x}_F, \widetilde{C}^F_i)}{\sigma_P(\mathbf{x}|d)}\right) + \frac{\sigma^2_P(\mathbf{x}|d) + (\mu_P(\mathbf{x}|d) - \mu_F(\mathbf{x}|d, \mathbf{x}_F, \widetilde{C}^F_i))^2}{2\sigma^2_F(\mathbf{x}|d, \mathbf{x}_F, \widetilde{C}^F_i)} - \frac{1}{2}. \end{aligned} \tag{3}$$

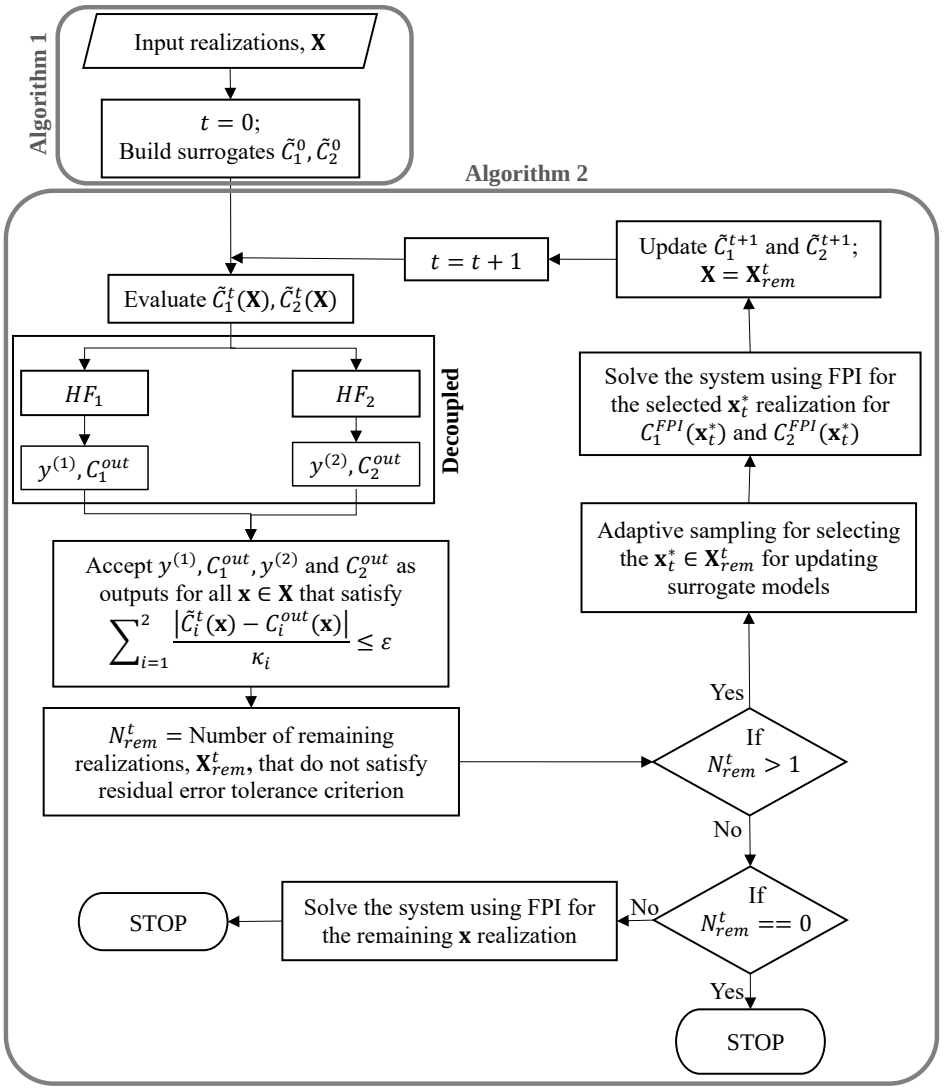

Figure 2. Multifidelity coupled uncertainty propagation method (HF_1 and HF_2 denotes high-fidelity analysis of disciplines 1 and 2, respectively, and t denotes the current cycle).

D_{KL} is used as the information gain metric. μ_P and σ_P are predictions from the present surrogate fit, and μ_F and σ_F are predictions from a possible future surrogate fit.

The total information gain at any $\mathbf{x}$ realization can be calculated by integrating over all possible values of $\widetilde{C}_i^F$ (defined by $G_P(\mathbf{x}_F|d)$) for $\mathbf{x}_F \in \mathbf{X}_{rem}^t$. Under the condition that the Kriging hyperparameters are fixed, one can derive a closed-form solution for calculating the total information gain to further reduce computational cost. Let the hyper-parameters of the present and future surrogates used for predicting G_P and G_F be the same. Then the prediction variance σ_F^2 is independent of the possible future value $\widetilde{C}_i^F$. Thus the KL divergence described in Equation 3 reduces to

$$
\begin{aligned}
&D_{KL}(G_P(\mathbf{x}|d) \parallel G_F(\mathbf{x}|d, \mathbf{x}_F, \widetilde{C}_i^F)) \\
&\quad = log\left(\frac{\sigma_F(\mathbf{x}|d, \mathbf{x}_F)}{\sigma_P(\mathbf{x}|d)}\right) + \frac{\sigma_P^2(\mathbf{x}|d) + (\mu_P(\mathbf{x}|d) - \mu_F(\mathbf{x}|d, \mathbf{x}_F, \widetilde{C}_i^F))^2}{2\sigma_F^2(\mathbf{x}|d, \mathbf{x}_F)} - \frac{1}{2} \\
&\quad = log\left(\frac{\sigma_F(\mathbf{x}|d, \mathbf{x}_F)}{\sigma_P(\mathbf{x}|d)}\right) + \frac{\sigma_P^2(\mathbf{x}|d) + \mu_P^2(\mathbf{x}|d) - 2\mu_P(\mathbf{x}|d)\mu_F(\mathbf{x}|d, \mathbf{x}_F, \widetilde{C}_i^F) + \mu_F^2(\mathbf{x}|d, \mathbf{x}_F, \widetilde{C}_i^F)}{2\sigma_F^2(\mathbf{x}|d, \mathbf{x}_F)} - \frac{1}{2}.
\end{aligned}
\tag{4}
$$

Integrating Equation 4 with respect to the Gaussian distribution of $\widetilde{C}_i^F$ (defined by $G_P(\mathbf{x}_F|d)$) to find the total information gain amounts to computing the expectation of the terms involving $\widetilde{C}_i^F$. Thus we only need

to compute $\mathbb{E}_{\widetilde{C}_i^F}[\mu_F(x|d, x_F, \widetilde{C}_i^F)]$ and $\mathbb{E}_{\widetilde{C}_i^F}[\mu_F^2(x|d, x_F, \widetilde{C}_i^F)]$. The rest of the terms in Equation 4 do not depend on $\widetilde{C}_i^F$. The total information gain at any realization $\mathbf{x}$ for the i^{th} coupling variable, $D_i(\mathbf{x}, \mathbf{x}_F)$, is given by

$$D_i(\mathbf{x}, \mathbf{x}_F) = \log\left(\frac{\sigma_F(\mathbf{x}|d, \mathbf{x}_F)}{\sigma_P(\mathbf{x}|d)}\right) + \frac{\sigma_P^2(\mathbf{x}|d) + \mu_P^2(\mathbf{x}|d) - 2\mu_P(\mathbf{x}|d)\mathbb{E}_i[\mu_F] + \mathbb{E}_i[\mu_F^2]}{2\sigma_F^2(\mathbf{x}|d, \mathbf{x}_F)} - \frac{1}{2}, \tag{5}$$

where $\mathbb{E}_i[\mu_F] = \mathbb{E}_{\widetilde{C}_i^F}\left[\mu_F(x|d, x_F, \widetilde{C}_i^F)\right]$ and $\mathbb{E}_i\left[\mu_F^2\right] = \mathbb{E}_{\widetilde{C}_i^F}\left[\mu_F^2(x|d, x_F, \widetilde{C}_i^F)\right]$ for ease of notation.

Since Kriging is a linear prediction model in observations Y, it is possible to calculate these expectations in closed-form. Here, Y is a $(N_{sur}+1)\times 1$ vector such that $Y^\top = [C_i^{FPI}(\mathbf{X}_{sur}^t), \widetilde{C}_i^F]^\top$ (with N_{sur} number of training points in d). The predictive mean can be written as

$$\mu_F(x|d, x_F, \widetilde{C}_i^F) = V^\top Y, \tag{6}$$

where V is a $(N_{sur}+1)\times 1$ vector. Thus the predictive mean can be decomposed in two parts as given by

$$\mu_F(x|d, x_F, \widetilde{C}_i^F) = V_{1:N_{sur}}^\top Y_{1:N_{sur}} + V_{N_{sur}+1}\widetilde{C}_i^F. \tag{7}$$

Now the expectations of the predicted mean and the square of the predicted mean from the future surrogate can be calculated as

$$\mathbb{E}_{\widetilde{C}_i^F}\left[\mu_F(\mathbf{x}|d, \mathbf{x}_F, \widetilde{C}_i^F)\right] = V_{1:N_{sur}}^\top Y_{1:N_{sur}} + V_{N_{sur}+1}\mu_P(\mathbf{x}|d), \tag{8}$$

$$\begin{aligned}\mathbb{E}_{\widetilde{C}_i^F}\left[\mu_F^2(\mathbf{x}|d, \mathbf{x}_F, \widetilde{C}_i^F)\right] &= (V_{1:N_{sur}}^\top Y_{1:N_{sur}})^2 + 2(V_{1:N_{sur}}^\top Y_{1:N_{sur}})V_{N_{sur}+1}\mu_P(\mathbf{x}|d) \\ &\quad + V_{N_{sur}+1}^2\left[\sigma_P^2(\mathbf{x}|d) + \mu_P^2(\mathbf{x}|d)\right] \\ &= \mathbb{E}_{\widetilde{C}_i^F}^2\left[\mu_F(\mathbf{x}|d, \mathbf{x}_F, \widetilde{C}_i^F)\right] + V_{N_{sur}+1}^2\sigma_P^2(\mathbf{x}|d).\end{aligned} \tag{9}$$

Finally, the total information gain can be computed by substituting Equations 8 and 9 in Equation 5. Note that if one is using a black-box Kriging model with no access to the vector V required in the above equations, Gauss-Hermite quadrature can also be used to approximate the integral in Equation 4 with respect to the distribution of $\widetilde{C}_i^F$ for finding total information gain. The drawback of doing that is the substantial increase in computational effort because of having to refit the surrogate for each possible future data value given by the Gauss-Hermite quadrature points.

The optimization problem for finding $\mathbf{x}_t^*$ through the information-gain-based adaptive sampling criterion combines the information gain at all $\mathbf{x}_{rem_j} \in \mathbf{X}_{rem}^t$ for all N_C coupling variables, as defined by

$$\mathbf{x}_t^* = \underset{\mathbf{x}_F \in \mathbf{X}_{rem}^t}{\operatorname{argmax}} \sum_{i=1}^{N_C}\sum_{j=1}^{N_{rem}^t} D_i(\mathbf{x}_{rem_j}|\mathbf{x}_F). \tag{10}$$

3. Maximum Weighted Information Gain

The weighted information gain criterion uses the present normalized residual error at $\mathbf{x}_F \in \mathbf{X}_{rem}^t$ as the weight for the information gain. The weight at $\mathbf{x}_F$ for the current cycle t is defined by

$$W_F^t(\mathbf{x}_F) = \frac{e^t(\mathbf{x}_F)}{\sum_{m=1}^{N_{rem}^t} e^t(\mathbf{x}_{rem_m})}, \tag{11}$$

where $\mathbf{x}_{rem_m} \in \mathbf{X}_{rem}^t$ and $e^t(\mathbf{x})$ is given by Equation 1. This attaches more importance to the input realizations that have higher associated residual errors. The optimization problem for the weighted information gain-based adaptive sampling strategy is given by

$$\mathbf{x}_t^* = \underset{\mathbf{x}_F \in \mathbf{X}_{rem}^t}{\operatorname{argmax}}\, W_F^t(\mathbf{x}_F)\sum_{i=1}^{N_C}\sum_{j=1}^{N_{rem}^t} D_i(\mathbf{x}_{rem_j}|\mathbf{x}_F). \tag{12}$$

C. Convergence Analysis

In general, the performance of the proposed algorithm is defined by the rate of convergence of the coupling variables, which affects the number of high-fidelity simulations. The rate of convergence will depend on the fidelity of the approximation being used. However, some statements on the convergence properties of the proposed multifidelity coupled uncertainty propagation algorithm can be made under certain conditions.

The first property to note is that the algorithm terminates in finite number of cycles. For any $\varepsilon \geq 0$ and $\forall \mathbf{x} \in \mathbf{X}, \exists t \leq N_{total} - N_{sur}$, such that $e^t(\mathbf{x}) \leq \varepsilon$. Thus, in the worst case scenario all $N_{total} - N_{sur}$ realizations undergo FPI, which implies that $t = N_{total} - N_{sur}$. However, as we show in the results, if approximations with appropriate fidelity and an intelligent adaptive update strategy are used, the number of cycles is typically much less than $N_{total} - N_{sur}$. The number of cycles depends on the quality of surrogate and the adaptive sampling strategy.

In order to explain the other convergence properties of the proposed algorithm, we need to first define FPI convergence. For a given realization $\mathbf{x} \in \mathbf{X}$, the iterating function on which FPI is implemented in this work is given by

$$F(C_1, \ldots, C_{N_C}) = \begin{pmatrix} H_{C_1}(C_1, \ldots, C_{N_C}, \mathbf{x}) \\ \vdots \\ H_{C_{N_C}}(C_1, \ldots, C_{N_C}, \mathbf{x}) \end{pmatrix}. \tag{13}$$

Then FPI proceeds through iterations defining

$$\begin{pmatrix} C_1^k \\ \vdots \\ C_{N_C}^k \end{pmatrix} = F(C_1^{k-1}, \ldots, C_{N_C}^{k-1}), \tag{14}$$

where k denotes the iteration number for FPI. FPI iterates till it converges to a fixed point depending on the error threshold for FPI, ε_{FPI}, when

$$\sum_{i=1}^{N_C} \frac{\left|C_i^k - C_i^{k-1}\right|}{\kappa_i} < \varepsilon_{FPI}, \tag{15}$$

where κ_i are normalization constants for coupling variables $i = 1, \ldots, N_C$.

The second property of our multifidelity coupled uncertainty propagation approach is that the algorithm converges pointwise to an FPI solution of the coupling variable for the case when $\varepsilon < \varepsilon_{FPI}$. For any given $\mathbf{x} \in \mathbf{X}$ and all coupling variables $i = 1, \ldots, N_C$, let $C_i^\varepsilon(\mathbf{x}) = C_i^{out}(\mathbf{x})$ when $e^t(\mathbf{x}) = \sum_{i=1}^{N_C} \frac{\left|\widetilde{C}_i^t(\mathbf{x}) - C_i^{out}(\mathbf{x})\right|}{\kappa_i} \leq \varepsilon$. Then it can be shown that $C_i^\varepsilon(\mathbf{x})$ converges pointwise to $C_i^{FPI}(\mathbf{x})$ when $\varepsilon < \varepsilon_{FPI}$. For accepted coupled variable output $C_i^\varepsilon(\mathbf{x})$, we have that $e^t(\mathbf{x}) \leq \varepsilon$, which implies that

$$\begin{aligned} \sum_{i=1}^{N_C} \frac{\left|\widetilde{C}_i^t(\mathbf{x}) - C_i^\varepsilon(\mathbf{x})\right|}{\kappa_i} &\leq \varepsilon < \varepsilon_{FPI} \\ \text{or, } \sum_{i=1}^{N_C} \frac{\left|\widetilde{C}_i^t(\mathbf{x}) - H_{C_i}(\widetilde{C}_1^t(\mathbf{x}), \ldots, \widetilde{C}_{N_C}^t(\mathbf{x}), \mathbf{x})\right|}{\kappa_i} &< \varepsilon_{FPI}. \end{aligned} \tag{16}$$

This is equivalent to satisfying the convergence criterion to a fixed point through FPI as given by Equation 15, which implies that $C_i^\varepsilon(\mathbf{x}) = C_i^{FPI}(\mathbf{x}), \forall i = 1, \ldots, N_C$ and $\forall \mathbf{x} \in \mathbf{X}$ when $\varepsilon < \varepsilon_{FPI}$. Note that multiple fixed points can exist for a given ε_{FPI} depending on the initial guess. Here, the fixed point solution obtained by FPI with initial guess $\widetilde{C}_i^t$ is used as the reference to compare to the solution of the proposed algorithm (where the solution is accepted in cycle t).

The third property of our approach is that, for any finite $\varepsilon \geq 0$, an upper bound on the error of the accepted solution from the algorithm, $C_i^\varepsilon(\mathbf{x})$, compared to an FPI solution, $C_i^{FPI}(\mathbf{x})$, can be established when $F(C_1, \ldots, C_{N_C})$ is assumed to be a contraction. Note that FPI convergence is guaranteed according to Banach fixed point theorem only when the iterating function is a contraction.[35,36] In metric space (M, d)

with a set M and a metric d on M, a function, say $f : M \to M$, is a contraction if there exists a Lipschitz constant $\gamma \in [0, 1)$ of f such that for all u and v in M,

$$d(f(u), f(v)) \leq \gamma d(u, v). \tag{17}$$

In this work, the metric d is defined by a normalized absolute difference of vectors u and v with m elements as given by

$$d(u, v) = \sum_{i=1}^{m} \frac{|u_i - v_i|}{\kappa_i}, \tag{18}$$

where κ_i is a normalization constant for i^{th} element of the vectors. Thus, the iterating function in Equation 13 can be defined to be a contraction if there exists a Lipschitz constant $\gamma \in [0, 1)$ such that

$$\sum_{i=1}^{N_C} \frac{\left|C_i^{k+1} - C_i^k\right|}{\kappa_i} \leq \gamma \sum_{i=1}^{N_C} \frac{\left|C_i^k - C_i^{k-1}\right|}{\kappa_i}. \tag{19}$$

For a contraction and a given $\varepsilon_{FPI} > 0$, $\exists N_F \in \mathbb{N}$ such that the FPI convergence criterion $\sum_{i=1}^{N_C} \frac{\left|C_i^{N_F} - C_i^{N_F-1}\right|}{\kappa_i} < \varepsilon_{FPI}$ (defined in Equation 15) is satisfied for all coupling variables starting with $\widetilde{C}_i^t(\mathbf{x})$ as the initial guess. Note that N_F is implicitly dependent on ε_{FPI} and ε in this case.

Then for any $\varepsilon \geq 0$, when the acceptance criterion $\sum_{i=1}^{N_C} \frac{\left|\widetilde{C}_i^t(\mathbf{x}) - C_i^{out}(\mathbf{x})\right|}{\kappa_i} \leq \varepsilon$ is met, i.e., $C_i^{\varepsilon}(\mathbf{x}) = C_i^{out}(\mathbf{x})$, it can be shown that $\sum_{i=1}^{N_C} \frac{\left|C_i^{FPI}(\mathbf{x}) - C_i^{\varepsilon}(\mathbf{x})\right|}{\kappa_i} \leq \frac{\gamma(1-\gamma^{N_F-1})}{1-\gamma}\varepsilon$, for all $\mathbf{x} \in \mathbf{X}$.

The solution from the proposed algorithm is compared to the fixed point obtained by starting with an initial guess of $C_i^0 = \widetilde{C}_i^t$, where the solution is accepted in cycle t. Then the coupled variable output after first iteration is $C_i^{out} = C_i^{\varepsilon}$ and is represented by C_i^1, where the numbers in the superscript refer to the iteration number for FPI. Then for contracting functions defined by Equation 19, it can be shown that

$$\begin{aligned}
\sum_{i=1}^{N_C} \frac{\left|C_i^2 - C_i^1\right|}{\kappa_i} &\leq \gamma \sum_{i=1}^{N_C} \frac{\left|C_i^1 - C_i^0\right|}{\kappa_i} \\
\sum_{i=1}^{N_C} \frac{\left|C_i^3 - C_i^2\right|}{\kappa_i} &\leq \gamma^2 \sum_{i=1}^{N_C} \frac{\left|C_i^1 - C_i^0\right|}{\kappa_i} \\
&\vdots \\
\sum_{i=1}^{N_C} \frac{\left|C_i^{N_F} - C_i^{N_F-1}\right|}{\kappa_i} &\leq \gamma^{N_F-1} \sum_{i=1}^{N_C} \frac{\left|C_i^1 - C_i^0\right|}{\kappa_i},
\end{aligned} \tag{20}$$

where $C_i^{N_F}$ is an FPI solution C_i^{FPI} for $i = 1, \ldots, N_C$.[35,36] Note that the superscripts for γ in Equation 20 refer to exponents.

Summing the left and right hand side of Equation 20, we get

$$\begin{aligned}
\sum_{i=1}^{N_C} \frac{\left|C_i^2 - C_i^1\right| + \cdots + \left|C_i^{N_F} - C_i^{N_F-1}\right|}{\kappa_i} &\leq (\gamma + \gamma^2 + \cdots + \gamma^{N_F-1}) \sum_{i=1}^{N_C} \frac{\left|C_i^0 - C_i^1\right|}{\kappa_i} \\
&= \frac{\gamma(1-\gamma^{N_F-1})}{1-\gamma} \sum_{i=1}^{N_C} \frac{\left|C_i^0 - C_i^1\right|}{\kappa_i}.
\end{aligned} \tag{21}$$

Using the triangle inequality on the left hand side of Equation 21, we get an upper bound on the error

compared to an FPI solution as given by

$$\sum_{i=1}^{N_C} \frac{\left|C_i^{N_F} - C_i^1\right|}{\kappa_i} \leq \frac{\gamma(1-\gamma^{N_F-1})}{1-\gamma} \sum_{i=1}^{N_C} \frac{\left|C_i^0 - C_i^1\right|}{\kappa_i} = \frac{\gamma(1-\gamma^{N_F-1})}{1-\gamma} \sum_{i=1}^{N_C} \frac{\left|\widetilde{C}_i^t - C_i^\varepsilon\right|}{\kappa_i}$$
$$\leq \frac{\gamma(1-\gamma^{N_F-1})}{1-\gamma}\varepsilon \tag{22}$$
$$\text{or, } \sum_{i=1}^{N_C} \frac{\left|C_i^{FPI} - C_i^\varepsilon\right|}{\kappa_i} \leq \frac{\gamma(1-\gamma^{N_F-1})}{1-\gamma}\varepsilon.$$

Note that for $\varepsilon < \varepsilon_{FPI}$, the FPI converges in one iteration, i.e., $N_F = 1$. This reduces the upper bound to 0 and this property boils down to $C_i^\varepsilon(\mathbf{x}) = C_i^{FPI}(\mathbf{x}), \forall i = 1, \ldots, N_C$ and $\forall \mathbf{x} \in \mathbf{X}$, which recovers the pointwise convergence of our method's second convergence property. The second convergence property is a special case of the third one.

In summary, the use of adaptive surrogate refinement means that under certain conditions, our method recovers the results that would be obtained using high-fidelity FPI on all samples. Yet, as the results in the next section show, the method can lead to significant reductions in computational cost.

IV. Numerical Experiments

In this section, numerical experiments are presented analyzing the three adaptive sampling strategies for the multifidelity coupled uncertainty propagation method on an analytic test problem, a fire detection satellite model analysis, and a wing aero-structural analysis. The developed method is compared to Monte Carlo simulation with FPI for every realization.

A. Analytic Test Problem

1. Problem setup

The analytic test problem used in this work has five input random variables and two coupling variables as seen in Figure 3. Each input random variable is modeled as being normally distributed with a mean of 1 and standard deviation of 0.1. This problem uses $\kappa_1 = 6.6259$ and $\kappa_2 = 7.5370$ as the normalization constants for the residual errors, where these values correspond to the multidisciplinary feasible solution for the coupling variables at the mean of the input random variables. The residual error tolerance, ε, is set at 1.5e-4. The number of iterations required for FPI convergence for the test problem is ~ 18 on average for $\varepsilon_{FPI} = 1.501e-4$. Thus, conducting Monte Carlo simulation with the embedded FPI is expensive.

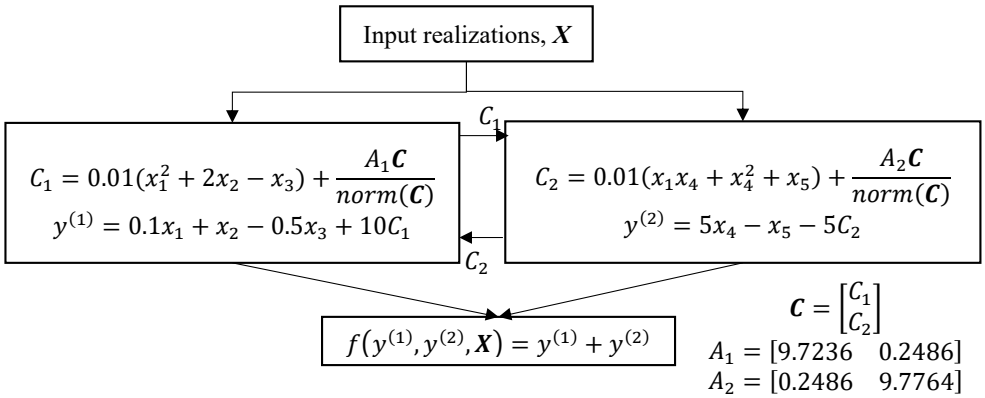

Figure 3. Analytic test problem

The efficiency of the multifidelity coupled uncertainty propagation method is assessed for total number of input realizations, N_{total}, values of 10^4 and 10^5, and an initial number of surrogate training samples, N_{sur}, value of 20, for the test problem. Each case is repeated 10 times with randomly generated Monte Carlo

samples in order to obtain statistics on the results. The three adaptive sampling strategies are abbreviated as *Max Res*, *Max IG* and *Max WIG* for maximum residual error, maximum information gain and maximum weighted information gain, respectively. The effect of surrogate accuracy on the algorithm performance is presented first, followed by a comparison of the different adaptive sampling strategies. Only the two feedback-coupled disciplines are considered for calculating the total number of high-fidelity simulations, since in a typical engineering problem the costs of the disciplinary analyses will dominate the cost of evaluating the system output.

2. *Accuracy of Surrogate*

The first test investigates the effect of global accuracy of the initial surrogate being used on the algorithm performance. Here, algorithm performance is quantified by the number of high-fidelity simulations used by the algorithm. The results are presented for the case of maximum residual error adaptive sampling criterion with $N_{total} = 10^4$. Two different trend functions for the Kriging surrogate are used: a constant and a linear polynomial (denoted by 'Max Res (constant trend)' and 'Max Res (linear trend)', respectively). The mean leave-one-out cross-validation error of the initial surrogate built with 20 samples (0^{th} cycle) from the 10 experiments is 0.0291 for Kriging with contant trend and 0.0063 for Kriging linear trend. The substantial difference in the accuracy of the initial surrogates leads to the superior performance of the more accurate surrogate, as seen Figure 4(a). Although the proposed algorithm using either surrogate performs better than Monte Carlo simulation with FPI, the more accurate Kriging model with linear trend clearly outperforms the other surrogate model. Kriging with linear trend leads to considerably fewer remaining samples after cycle 0, as seen in Figure 4(b), which in turn leads to fewer samples being passed through the remaining cycles and thus, higher efficiency of the overall uncertainty assessment. This indicates that it pays to invest in building a good quality initial surrogate. From here on, Kriging with linear trend is used as the surrogate for generating further results.

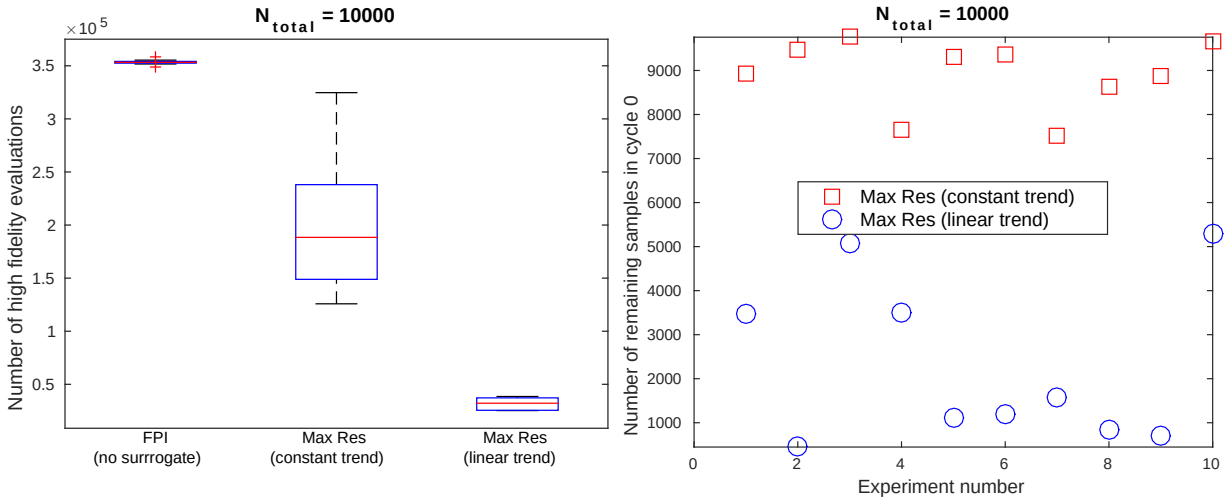

Figure 4. Effect of surrogate accuracy on the algorithm performance for analytic test problem for 10 experiments with $N_{total} = 10^4$: (a) boxplot showing performance of different surrogates compared to Monte Carlo simulation with FPI, and (b) number of remaining samples after using initial surrogate in cycle 0 for each of the 10 experiments.

3. *Comparison of Adaptive Sampling Strategies*

Table 1 presents the results for the comparison of different adaptive sampling strategies and Monte Carlo simulation with FPI for the test problem. For both $N_{total} = 10^4$ and 10^5, the results indicate that all adaptive sampling strategies lead to a reduction of more than 90% (averaged over 10 experiments) in the total number of high-fidelity simulations required (considering both the disciplines) as compared to using standard Monte Carlo simulation with FPI. The residual error and weighted information gain strategies perform almost

equally well and better than the information gain strategy on average over the 10 experiments, as seen from Table 1. Figure 5 shows similar performance for the three different adaptive sampling strategies, with the information gain strategy performing slightly worse than the other two. However, if the performance for each individual experiment is analyzed as shown in Figure 6, it reveals that in $\sim 30\%$ of experiments for $N_{total} = 10^4$ and $\sim 50\%$ of experiments for $N_{total} = 10^5$, information gain performs similar or outperforms the residual error strategy. This gives more credence to the use of a combined strategy in the form of weighted information gain. The weighted information gain strategy achieves a good balance between the residual error and information gain strategies in most cases, while usually being biased towards the better option as seen in Figure 6 ($\sim 80\%$ of the cases).

Table 1. Comparison of efficiency of different adaptive sampling strategies and Monte Carlo simulation with FPI for analytic test problem.

N_{total}	Sampling strategy	Total number of cases for FPI		Number of high-fidelity simulations	
		Mean	Standard deviation	Mean	Standard deviation
10^4 (10 experiments)	Monte Carlo simulation with FPI	10^4	–	353,414	2,456
	Max Res	37.8	3.7	31,656 (-91%)	5,614
	Max IG	41.1	3.3	33,455 (-90.5%)	7,226
	Max WIG	38.5	2.6	32,318 (-90.9%)	6,730
10^5 (10 experiments)	Monte Carlo simulation with FPI	10^5	–	3,545,391	5,600
	Max Res	50.1	4.7	341,008 (-90.4%)	71,805
	Max IG	56.1	7.4	343,812 (-90.3%)	71,498
	Max WIG	49.7	3.7	320,038 (-91%)	52,103

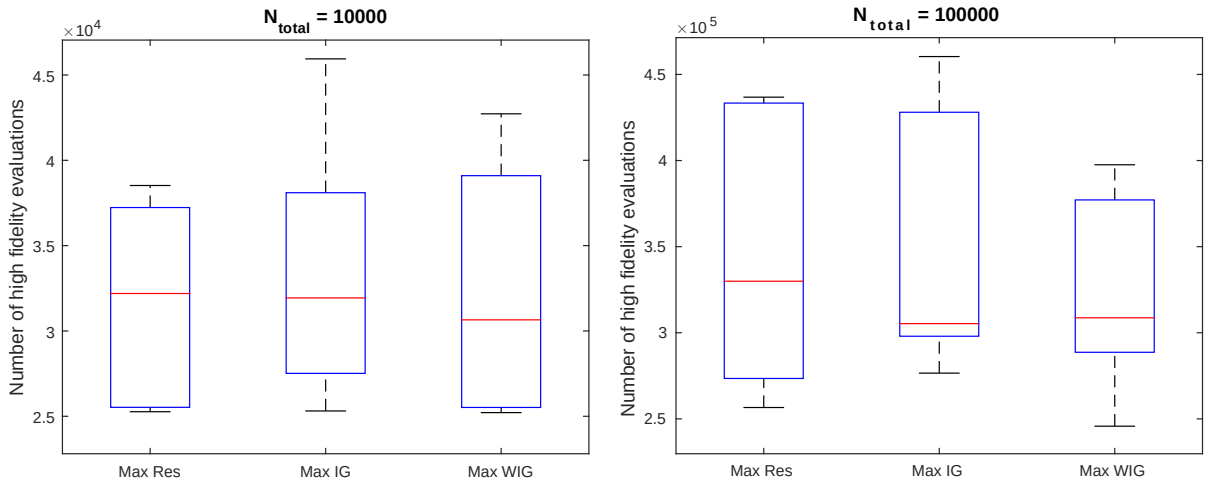

Figure 5. Boxplot comparing performance of different adaptive sampling strategies for analytic test problem for 10 experiments with (a) $N_{total} = 10^4$, and (b) $N_{total} = 10^5$.

Figure 7 shows a comparison of the empirical CDFs of the system output, f, predicted by the three adaptive sampling strategies and the empirical CDF of the FPI solution for a particular experiment with $N_{total} = 10^4$. Here, the fixed point is found by starting with the surrogate prediction of the coupled variable at the accepted cycle and for $\varepsilon_{FPI} = 1.501e4$. For all the experiments, the empirical CDF of the FPI solutions

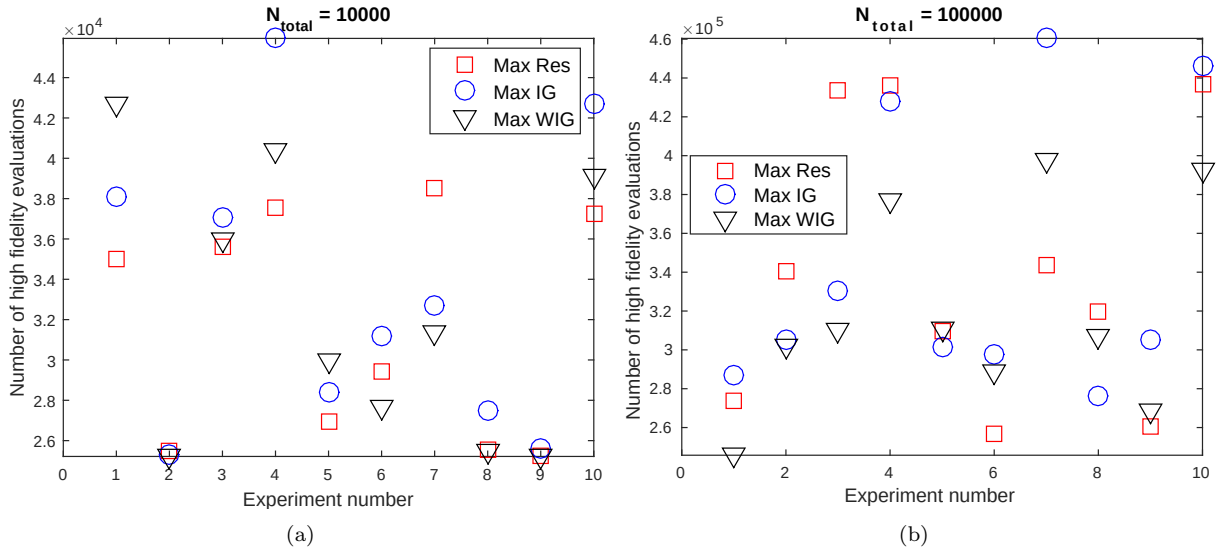

Figure 6. Performance for each of the 10 experiments for different adaptive sampling strategies for analytic test problem with (a) $N_{total} = 10^4$, and (b) $N_{total} = 10^5$.

match the empirical CDFs predicted by the three adaptive sampling strategies. This follows naturally from the pointwise convergence property of our approach, since $\varepsilon < \varepsilon_{FPI}$ in this case.

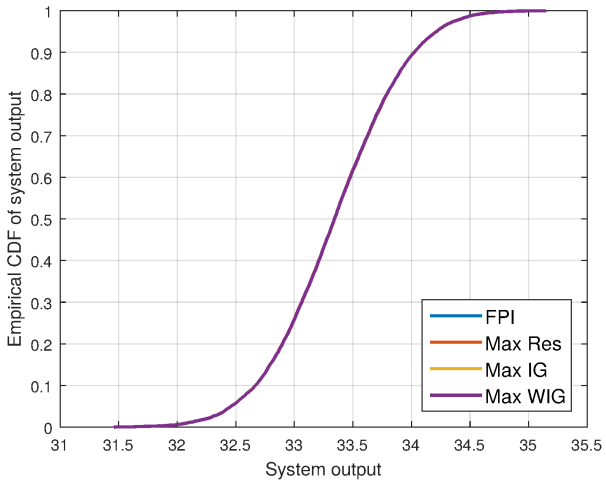

Figure 7. Comparison of empirical CDFs of the system output predicted by the three adaptive sampling strategies to the empirical CDF evaluated using Monte Carlo simulation with FPI solution for analytic test problem with $N_{total} = 10^4$.

The convergence of the algorithm in terms of the number of remaining realizations, N_{rem}^t, that did not satisfy the residual error tolerance after each cycle is shown in Figure 8. All the strategies have similar convergence rates. The number of cases of FPI executions is similar for the residual error and weighted information gain adaptive sampling strategies as seen in Table 1. A comparison of the number of cases of FPI executions for samples sizes of 10^4 and 10^5 indicates only a small increase for the higher sample size. This indicates an increase in efficiency of the proposed method as the number of samples increases. In all the cases, the number of realizations where FPI is employed in the multifidelity coupled uncertainty propagation method is successfully decreased ($\ll N_{total}$) as seen in Table 1.

Figures 9 to 11 show the progress of the algorithm through a slice of the design space (input random variables x_1 and x_2). The figures show the accepted realizations and sampling locations according to the choice of adaptive sampling strategy for selective cycles for the test problem for $N_{total} = 10^4$. "Initial

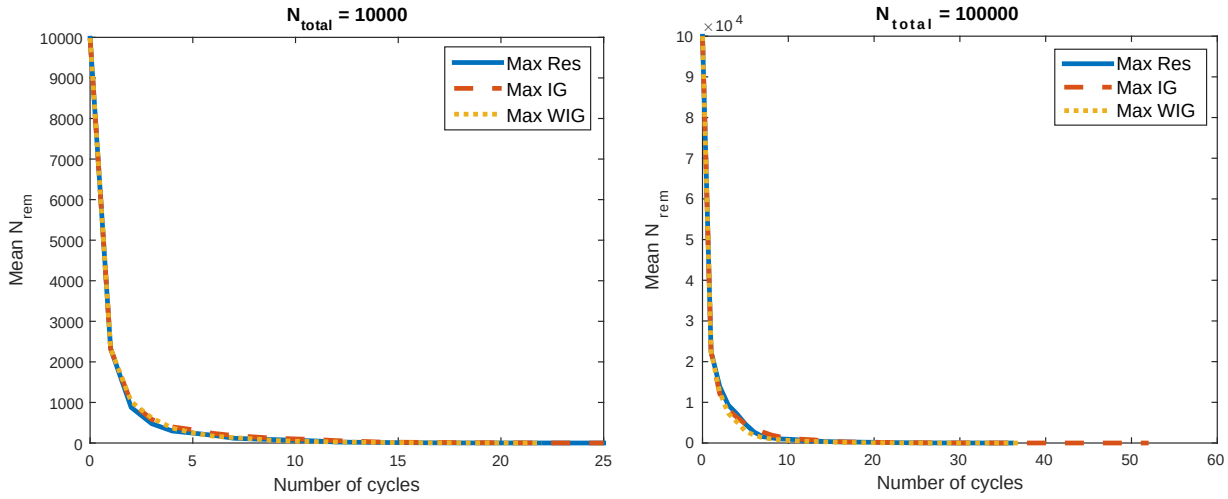

Figure 8. Number of realizations of X that do not satisfy the error tolerance after each cycle for analytic test problem with (a) $N_{total} = 10^4$, and (b) $N_{total} = 10^5$.

samples" refers to all the samples in $\mathbf{X}$, "Accepted samples" refer to the set of all those samples for which the residual error tolerance criterion is satisfied after that cycle, "Adaptive sampling location" refers to $\mathbf{x}_t^*$, and "FPI locations" refers to all those samples where FPI is used in order to get the true values of coupling variables to build or refine the surrogates.

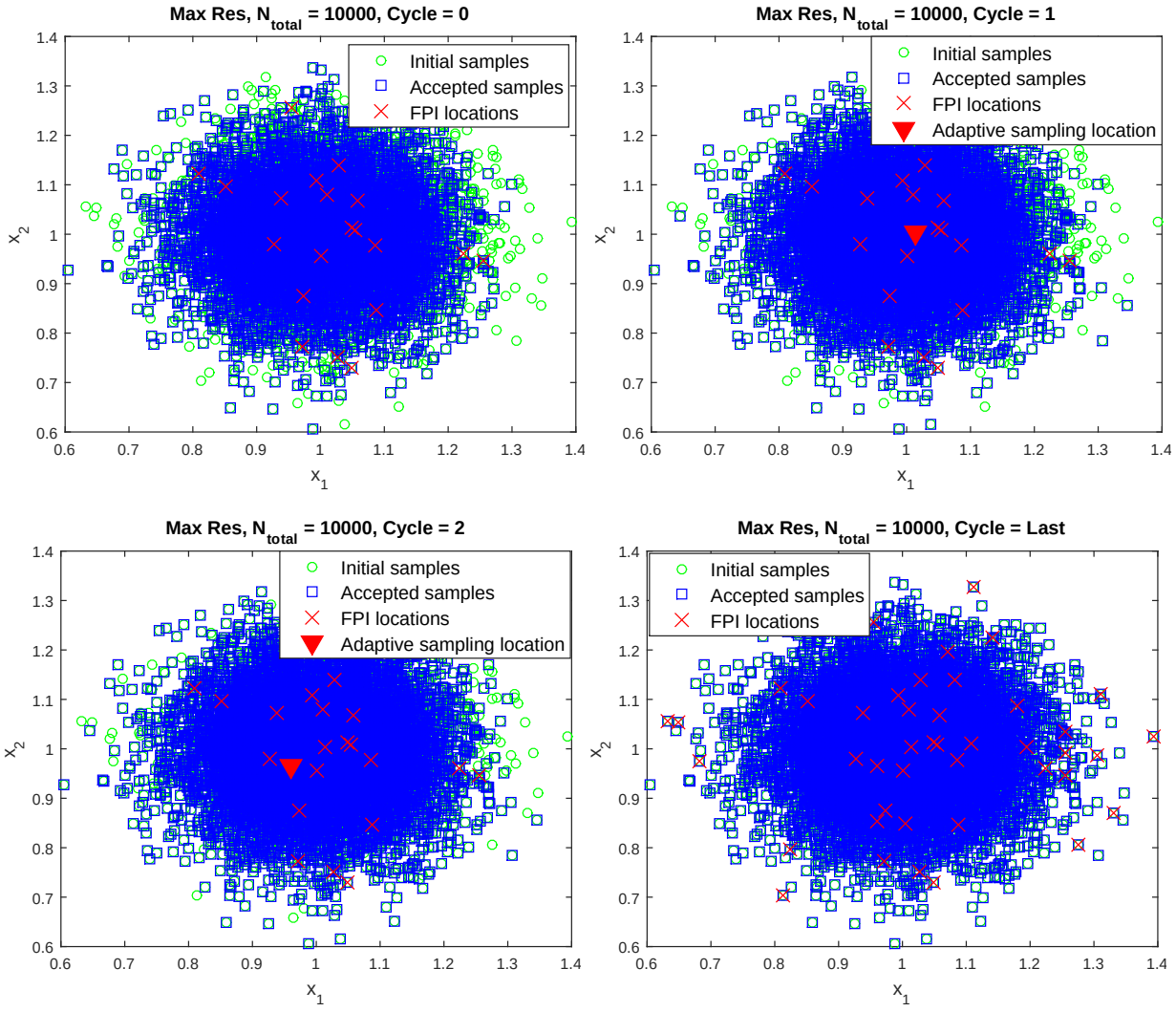

Figure 9. A slice of the design space showing the spread of accepted and remaining X realizations with the maximum residual error adaptive sampling location for selected cycles for analytic test problem.

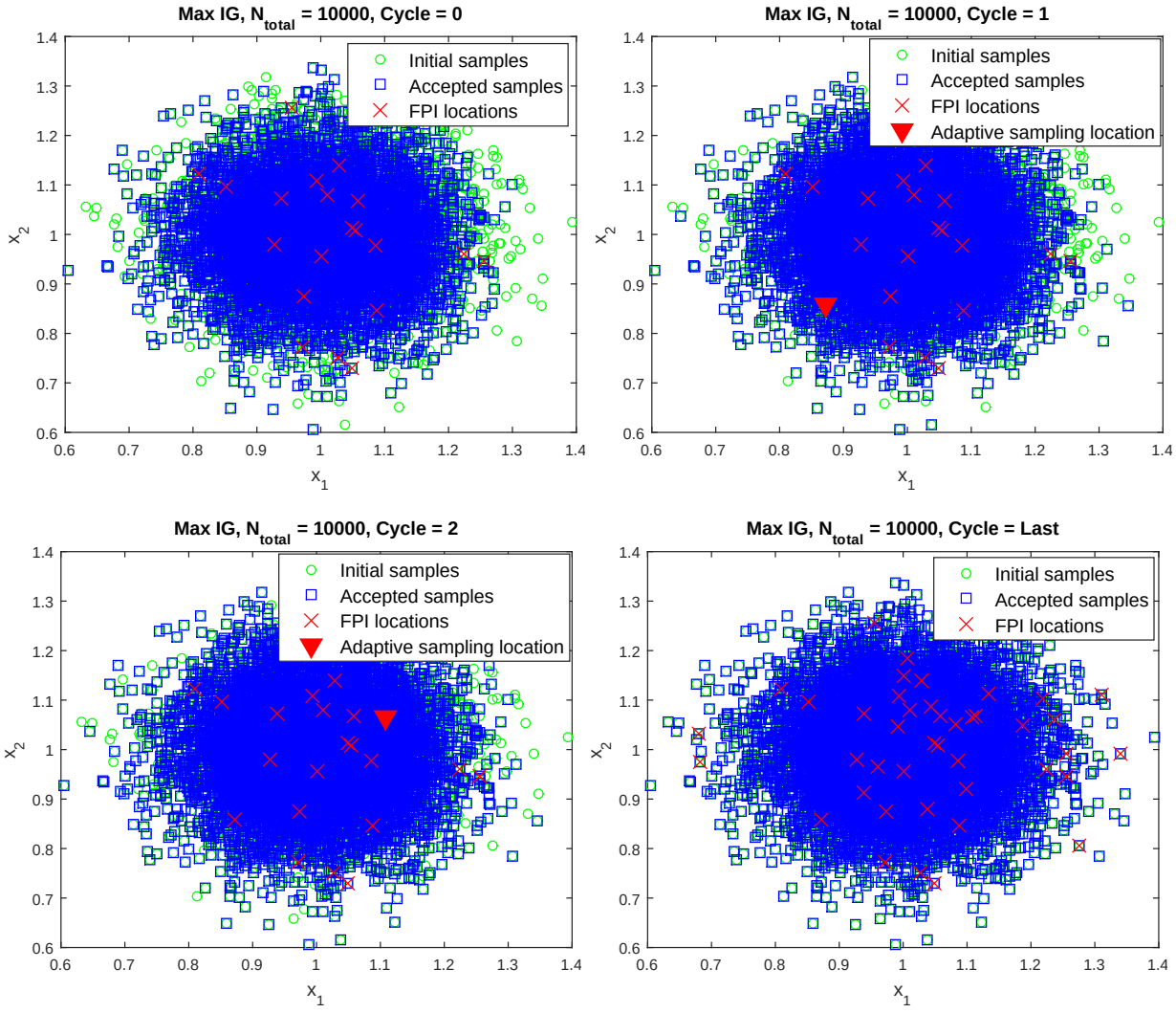

Figure 10. A slice of the design space showing the spread of accepted and remaining X realizations with the maximum information gain adaptive sampling location for selected cycles for analytic test problem.

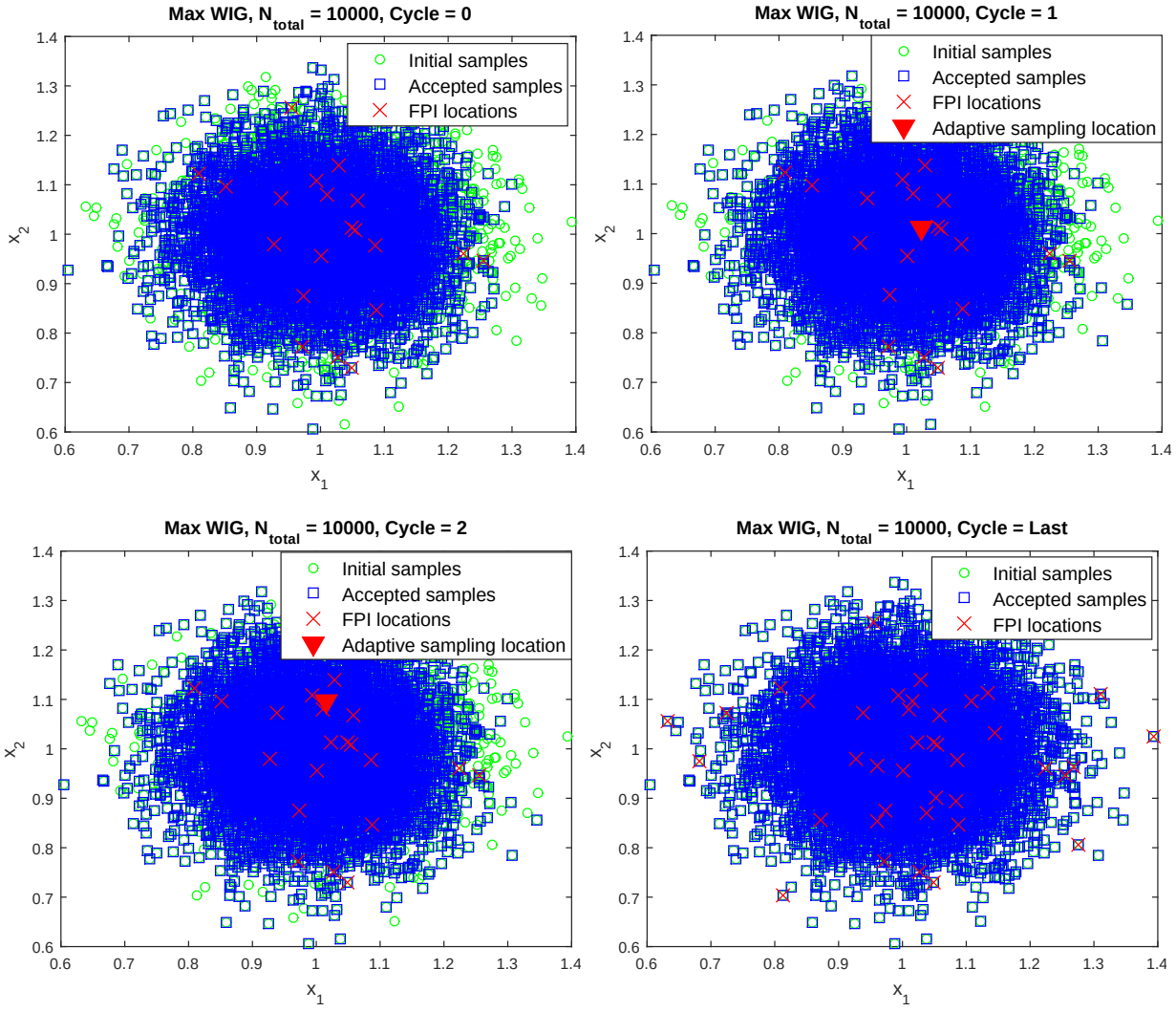

Figure 11. A slice of the design space showing the spread of accepted and remaining X realizations with the maximum weighted information gain adaptive sampling location for selected cycles for analytic test problem.

B. Fire Detection Satellite Model

The performance of the multifidelity coupled uncertainty propagation method is analyzed on a three-discipline satellite model originally described in Ref. 10 and presented in the context of robust optimization in Ref. 11. Figure 12 illustrates the fire detection satellite model and the five random inputs we used for this problem. The three disciplines (orbit analysis, attitude control, and power analysis) exchange information through feed-forward and feedback coupling. More detail about the physics models describing each analysis can be found in Ref. 11.

The five uncertain input random variables that represent the uncertainty in the system are defined as Gaussian random variables with mean and standard deviation as shown in Table 3. The surrogates are built for the feedback coupling variables, the power for the attitude control system (P_{ACS}) and the moments of inertia (I_{max}, and I_{min}), defining the interaction between the attitude control and power analysis disciplines. The total torque (τ_{tot}), total power (P_{tot}) and area of solar array (A_{sa}) are the system outputs that are analyzed in this work. This problem uses $\kappa_{P_{ACS}} = 130, \kappa_{I_{max}} = 6600$, and $\kappa_{I_{min}} = 5100$ as the normalization constants for the residual errors, where these values correspond to the multidisciplinary feasible solution for the coupling variables at the mean of the input random variables. The residual error tolerance, ε, is set at 1.5e-2. The number of iterations required for FPI convergence for the test problem is approximately three on average for $\varepsilon_{FPI} = 1.501e-2$. The method is tested for total number of input realizations, $N_{total} = 10^5$, and an initial number of surrogate training samples, $N_{sur} = 40$. Note that the orbital analysis needs to be executed only N_{total} times (independent of the feedback coupled disciplines) since it is only feed-forward coupled with the other two disciplines. All three disciplines are considered when calculating the total number of high-fidelity simulations.

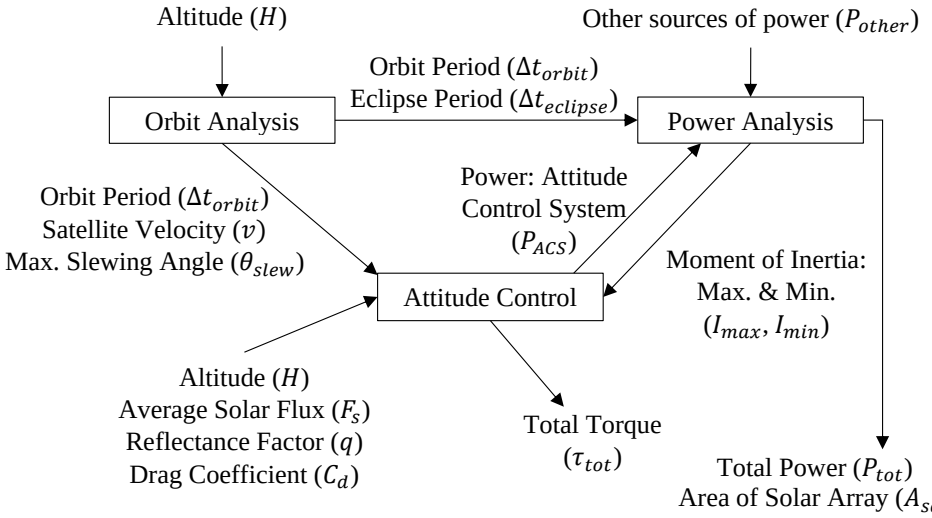

Figure 12. Multidisciplinary coupled system representing the fire detection satellite problem from Ref. 10,11.

Table 4 presents the results for the comparison of different adaptive sampling strategies and Monte Carlo simulation with FPI for the satellite problem. The results indicate that all adaptive sampling strategies lead to a reduction of $53-54\%$ in the total number of high-fidelity simulations required (considering all the disciplines) as compared to using standard Monte Carlo simulation with FPI. The weighted information gain strategy is the most efficient for this problem. There is also significant reduction in the number of cases for which FPI is executed for all three adaptive sampling strategies. We note that for this case the number of cases for which FPI is executed is reduced by a factor of $> 99\%$, but the number of high-fidelity simulations is reduced only by a factor of $53-54\%$. This disparity is due to the relatively low number of iterations required to reach the fixed point for this problem (three iterations on average) and the need to execute additional high-fidelity simulations in our accept/reject decisions and our adaptive surrogate updates.

Figure 13 shows a comparison of the empirical CDFs of the system outputs, τ_{tot}, P_{tot}, andA_{sa}, predicted by the three adaptive sampling strategies and the empirical CDF of the FPI solution for a particular experiment with $N_{total} = 10^5$. The fixed point is found by starting with the surrogate prediction of the coupled variable at the accepted cycle. For all the experiments, the empirical CDF of the FPI solutions match the

Table 2. Deterministic inputs for fire detection satellite model.

Variable	Symbol	Unit	Numerical Value
Earth's radius	R_E	m	6,378,140
Gravitational parameter	μ	m^3s^{-2}	3.986 x 10^{14}
Target diameter	ϕ_{target}	m	235,000
Light speed	c	ms^{-1}	2.9979 x 10^8
Area reflecting radiation	A_s	m^2	13.85
Sun incidence angle	i	deg	0
Slewing time period	Δt_{slew}	s	760
Magnetic moment of earth	M	A m^2	7.96 x 10^{15}
Atmospheric density	q	kg m^{-3}	5.1480 x 10^{11}
Cross-sectional in flight direction	A	m^2	13.85
No. of reaction wheels	n	–	3
Maximum velocity of a wheel	ω_{max}	rpm	6000
Holding power	P_{hold}	W	20
Inherent degradation of array	I_d	–	0.77
Power efficiency	η	–	0.22
Lifetime of spacecraft	LT	Years	15
Degradation in power production capability	ϵ_{deg}	% per year	0.0375
Length to width ratio of solar array	r_{lw}	–	3
Number of solar arrays	n_{sa}	–	3
Average mass density to arrays	ρ_{sa}	kg m^3	700
Thickness of solar panels	t	m	0.005
Distance between panels	D	m	2
Moments of inertia of spacecraft body	I_{body}	kg m^2	$I_{body,X} = I_{body,Y} = 6200; I_{body,Z} = 4700$
Deviation of moment axis from vertical	θ	deg	15
Moment arm: solar radiation torque	L_{sp}	m	2
Residual dipole	R_D	A m^2	5
Moment arm: aerodynamic torque	L_a	m	2

Table 3. Uncertain input random variables for fire detection satellite model.

Variable	Symbol	Unit	Mean	Standard deviation
Altitude	H	m	18,000,000	1,000,000
Average solar flux	F_s	W/m^2	1400	20
Reflectance factor	q	–	0.5	1
Drag coefficient	C_d	–	1	0.3
Other power sources	P_{other}	W	1000	50

Table 4. Comparison of efficiency of different adaptive sampling strategies and Monte Carlo simulation with FPI for fire detection satellite problem.

N_{total}	Sampling strategy	Total number of cases for FPI	Number of high-fidelity simulations
10^5	Monte Carlo simulation with FPI	10^5	697,462
	Max Res	66	324,120 (-53.5%)
	Max IG	73	321,660 (-53.9%)
	Max WIG	60	320,836 (-54%)

empirical CDFs predicted by the three adaptive sampling strategies for all the system outputs. Similar to the analytic test problem, this follows from the pointwise convergence property of our approach, since $\varepsilon < \varepsilon_{FPI}$ in this case.

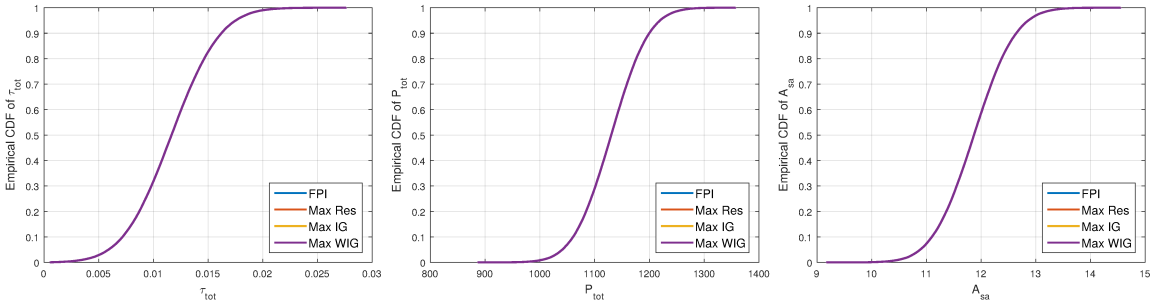

(a) (b) (c)

Figure 13. Comparison of empirical CDFs of system outputs for the fire detection satellite problem predicted by the three adaptive sampling strategies to the empirical CDF evaluated using Monte Carlo simulation with FPI solution for $N_{total} = 10^5$.

C. Aero-Structural Analysis of Wing

The multifidelity coupled uncertainty propagation method is applied to a coupled aero-structural analysis of a wing (Figure 14). The aerodynamics analysis uses a vortex lattice method expanded from a modern adaptation of Prandtl's classic lifting line theory.[37] The structural analysis uses a linear 6-DOF-per-element spatial beam model. The coupled aero-structural analysis code (OpenAeroStruct[38,39]) is implemented on the OpenMDAO architecture.[40] In this case, seven spanwise points and two chordwise points are used to build the wing mesh and the wing is analyzed for Mach number 0.84. The variability in the Young's modulus (E) and the shear modulus (G) of the material used for the wing represent the uncertainty in the system. These input random variables are defined using truncated normal distributions with parameters described in Table 5. The feedback-coupled variables in this case are the loads and displacements ($N_C = 84$). This problem uses absolute value of the multidisciplinary feasible solution for the coupling variables at the mean of the input random variables as the normalization constants for the residual errors (note that if this calculated value is 0 then it is set to 1). The system outputs of interest are maximum forces in the x-y-z-directions (F_x, F_y, F_z), maximum moments in the y-z-directions (M_y, M_z), and maximum displacement in the z-direction (u_z).

The residual error tolerance, ε, is set at 1.5e-5. The number of iterations required for FPI convergence for the test problem is approximately five on average for $\varepsilon_{FPI} = 1.501e-5$. The method is tested for total number of input realizations, $N_{total} = 10^4$, and an initial number of surrogate training samples, $N_{sur} = 25$.

Table 6 presents the results for the comparison of different adaptive sampling strategies and Monte Carlo simulation with FPI for the aero-structural problem. The results indicate that all adaptive sampling strategies lead to a reduction of around 75% in the total number of high-fidelity simulations required (considering both disciplines) as compared to using standard Monte Carlo simulation with FPI. There is also signifi-

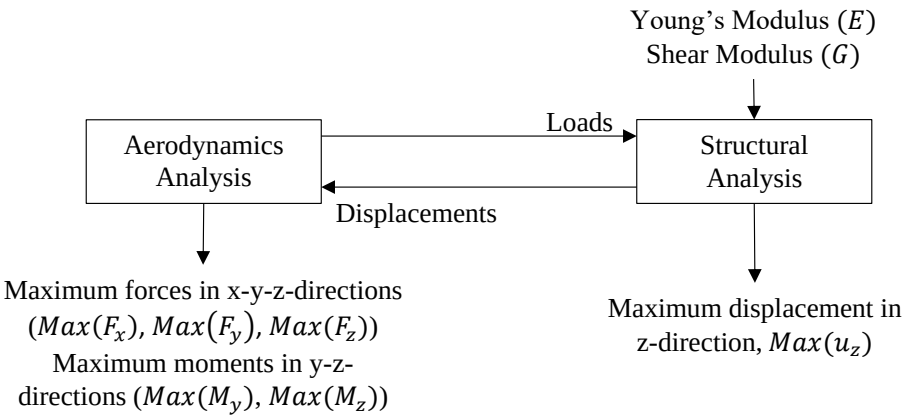

Figure 14. Multidisciplinary coupled system for wing aero-structural analysis.

Table 5. Uncertain input random variables for aero-structural wing analysis.

Variable	Symbol	Unit	Mean	Standard deviation	Lower bound	Upper bound
Young's Modulus	E	GPa	70	5	60	80
Shear Modulus	G	GPa	30	1	28	32

cant reduction in the number of cases for which FPI is executed for all three adaptive sampling strategies. The residual error strategy performs the best for this problem. The pointwise convergence property of our approach for the system outputs is also observed for this problem ($\varepsilon < \varepsilon_{FPI}$) as shown in Figure 15.

Table 6. Comparison of efficiency of different adaptive sampling strategies and Monte Carlo simulation with FPI for wing aero-structural analysis.

N_{total}	Sampling strategy	Total number of cases for FPI	Number of high-fidelity simulations
10^4	Monte Carlo simulation with FPI	10^4	100,000
	Max Res	31	24,322 (-75.7%)
	Max IG	33	25,354 (-74.6%)
	Max WIG	31	24,630 (-75.4%)

V. Concluding Remarks

This paper has developed a new multifidelity coupled uncertainty propagation method for feedback-coupled multidisciplinary systems. Instead of using fixed point iteration with Monte Carlo simulation for uncertainty propagation, the proposed method works to reduce the number of realizations for which FPI is employed. An essential feature of this method is that it maintains the same level of accuracy in the results as the original coupled high-fidelity system as shown through rigorous convergence analysis. Another advantage of the proposed method is the ability to partially decouple the process, which is helpful when communication between different disciplines is cumbersome, while preserving the accuracy of the mapping from the inputs to the system outputs.

The multifidelity coupled uncertainty propagation method uses surrogates to approximate the coupling variables and iteratively refines these surrogates using adaptive sampling strategies. An information-gain-based and a residual-error-based adaptive sampling strategy is explored in this work. The information gain weighted with the residual errors is used as another adaptive sampling strategy. For the test problem used in this work, a substantial decrease in the number of high-fidelity simulations as compared to Monte Carlo

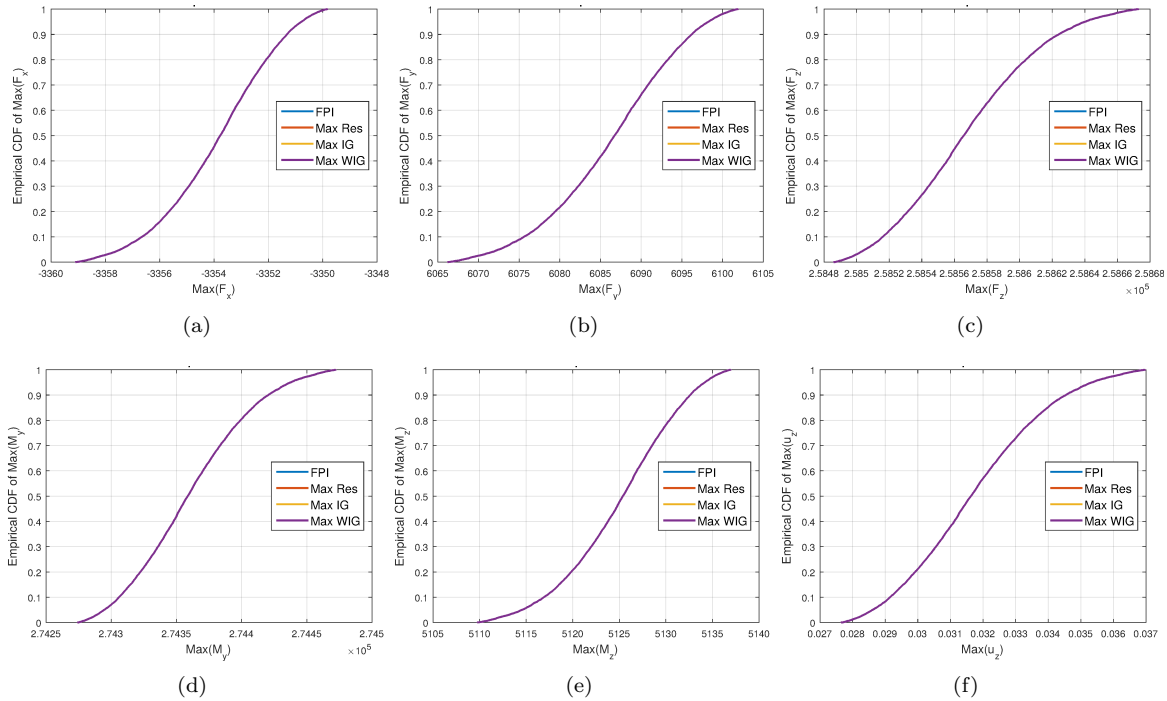

Figure 15. Comparison of empirical CDFs of system outputs predicted by the three adaptive sampling strategies to the empirical CDF evaluated using Monte Carlo simulation with FPI solution for the wing aero-structural analysis with $N_{total} = 10^4$.

simulation with FPI ($> 90\%$) is obtained for all the adaptive sampling strategies. The weighted information gain adaptive sampling strategy achieves a good balance by combining the residual error and information gain strategies. For all cases considered, the multifidelity coupled uncertainty propagation method successfully decreased the number of realizations where FPI is employed by more than 99% ($\ll N_{total}$). A decrease of more than 50% for the fire detection satellite problem and around 75% for the wing aero-structural analysis is achieved in the number of high-fidelity simulations. For both application problems, a significant decrease in total number of cases where FPI is employed is obtained by all three adaptive sampling strategies as compared to standard Monte Carlo simulation with FPI. For all three problems, the distributions for the system outputs is shown to converge pointwise to the solution obtained through Monte Carlo simulation with FPI under the given setting.

Acknowledgement

This work has been supported in part by the Air Force Office of Scientific Research (AFOSR) MURI on managing multiple information sources of multi-physics systems, Program Manager Jean-Luc Cambier, Award Number FA9550-15-1-0038. The authors also thank researchers at the University of Michigan Multidisciplinary Design Optimization Laboratory and at Texas A&M for providing and assisting in the setup of the aero-structural codes for wing analysis.

References

[1]Sobieszczanski-Sobieski, J. and Haftka, R. T., "Multidisciplinary aerospace design optimization: survey of recent developments," *Structural optimization*, Vol. 14, No. 1, 1997, pp. 1–23.

[2]Alexandrov, N. M. and Hussaini, M. Y., *Multidisciplinary design optimization: State of the art*, Vol. 80, SIAM, 1997.

[3]Martins, J. R. and Lambe, A. B., "Multidisciplinary design optimization: a survey of architectures," *AIAA journal*, Vol. 51, No. 9, 2013, pp. 2049–2075.

[4]Viana, F. A., Simpson, T. W., Balabanov, V., and Toropov, V., "Metamodeling in multidisciplinary design optimization: how far have we really come?" *AIAA Journal*, Vol. 52, No. 4, 2014, pp. 670–690.

[5]Yao, W., Chen, X., Luo, W., van Tooren, M., and Guo, J., "Review of uncertainty-based multidisciplinary design optimization methods for aerospace vehicles," *Progress in Aerospace Sciences*, Vol. 47, No. 6, 2011, pp. 450–479.

[6]Martin, J. D. and Simpson, T. W., "A methodology to manage system-level uncertainty during conceptual design," *Journal of Mechanical Design*, Vol. 128, No. 4, 2006, pp. 959–968.

[7]Amaral, S., Allaire, D., and Willcox, K., "A decomposition-based approach to uncertainty analysis of feed-forward multicomponent systems," *International Journal for Numerical Methods in Engineering*, Vol. 100, No. 13, 2014, pp. 982–1005.

[8]Culler, A. J. and McNamara, J. J., "Studies on fluid-thermal-structural coupling for aerothermoelasticity in hypersonic flow," *AIAA journal*, Vol. 48, No. 8, 2010, pp. 1721–1738.

[9]Hearn, T. A., Hendricks, E., Chin, J., and Gray, J. S., "Optimization of Turbine Engine Cycle Analysis with Analytic Derivatives," *17th AIAA/ISSMO Multidisciplinary Analysis and Optimization Conference*, 2016, p. 4297.

[10]Larson, W. J. and Wertz, J. R., "Space mission analysis and design," Tech. rep., Microcosm, Inc., Torrance, CA (US), 1992.

[11]Zaman, K. and Mahadevan, S., "Robustness-based design optimization of multidisciplinary system under epistemic uncertainty," *AIAA Journal*, Vol. 51, No. 5, 2013, pp. 1021–1031.

[12]Dunning, P., Kim, H., and Mullineux, G., "Introducing Loading Uncertainty in Topology Optimization," *AIAA Journal*, Vol. 49, No. 4, 2011, pp. 760–768.

[13]Cramer, E. J., Dennis, Jr, J., Frank, P. D., Lewis, R. M., and Shubin, G. R., "Problem formulation for multidisciplinary optimization," *SIAM Journal on Optimization*, Vol. 4, No. 4, 1994, pp. 754–776.

[14]Balling, R. J. and Sobieszczanski-Sobieski, J., "Optimization of coupled systems-A critical overview of approaches," *AIAA journal*, Vol. 34, No. 1, 1996, pp. 6–17.

[15]Alexandrov, N. M. and Kodiyalam, S., "Initial results of an MDO method evaluation study," *Proceedings of the 7th AIAA/USAF/NASA/ISSMO Symposium on Multidisciplinary Analysis and Optimization*, 1998.

[16]Arnst, M., Ghanem, R., Phipps, E., and Red-Horse, J., "Reduced chaos expansions with random coefficients in reduced-dimensional stochastic modeling of coupled problems," *International Journal for Numerical Methods in Engineering*, Vol. 97, No. 5, 2014, pp. 352–376.

[17]Arnst, M., Ghanem, R., Phipps, E., and Red-Horse, J., "Dimension reduction in stochastic modeling of coupled problems," *International Journal for Numerical Methods in Engineering*, Vol. 92, No. 11, 2012, pp. 940–968.

[18]Arnst, M., Soize, C., and Ghanem, R., "Hybrid sampling/spectral method for solving stochastic coupled problems," *SIAM/ASA Journal on Uncertainty Quantification*, Vol. 1, No. 1, 2013, pp. 218–243.

[19]Chen, X., Ng, B., Sun, Y., and Tong, C., "A flexible uncertainty quantification method for linearly coupled multi-physics systems," *Journal of Computational Physics*, Vol. 248, 2013, pp. 383–401.

[20]Jiang, Z., Li, W., Apley, D. W., and Chen, W., "A Spatial-Random-Process Based Multidisciplinary System Uncertainty Propagation Approach With Model Uncertainty," *Journal of Mechanical Design*, Vol. 137, No. 10, 2015, pp. 101402.

[21]Du, X. and Chen, W., "Collaborative reliability analysis under the framework of multidisciplinary systems design," *Optimization and Engineering*, Vol. 6, No. 1, 2005, pp. 63–84.

[22]Mahadevan, S. and Smith, N., "Efficient first-order reliability analysis of multidisciplinary systems," *International Journal of Reliability and Safety*, Vol. 1, No. 1-2, 2006, pp. 137–154.

[23]Sankararaman, S. and Mahadevan, S., "Likelihood-based approach to multidisciplinary analysis under uncertainty," *Journal of Mechanical Design*, Vol. 134, No. 3, 2012, pp. 031008.

[24]Jones, D. R., "A taxonomy of global optimization methods based on response surfaces," *Journal of global optimization*, Vol. 21, No. 4, 2001, pp. 345–383.

[25]Queipo, N. V., Haftka, R. T., Shyy, W., Goel, T., Vaidyanathan, R., and Tucker, P. K., "Surrogate-based analysis and optimization," *Progress in aerospace sciences*, Vol. 41, No. 1, 2005, pp. 1–28.

[26]Bichon, B. J., Eldred, M. S., Swiler, L. P., Mahadevan, S., and McFarland, J. M., "Efficient global reliability analysis for nonlinear implicit performance functions," *AIAA journal*, Vol. 46, No. 10, 2008, pp. 2459–2468.

[27]Basudhar, A. and Missoum, S., "Adaptive explicit decision functions for probabilistic design and optimization using support vector machines," *Computers & Structures*, Vol. 86, No. 19, 2008, pp. 1904–1917.

[28]Villemonteix, J., Vazquez, E., and Walter, E., "An informational approach to the global optimization of expensive-to-evaluate functions," *Journal of Global Optimization*, Vol. 44, No. 4, 2009, pp. 509–534.

[29]Hennig, P. and Schuler, C. J., "Entropy search for information-efficient global optimization," *The Journal of Machine Learning Research*, Vol. 13, No. 1, 2012, pp. 1809–1837.

[30]Hernández-Lobato, J. M., Hoffman, M. W., and Ghahramani, Z., "Predictive entropy search for efficient global optimization of black-box functions," *Advances in Neural Information Processing Systems*, 2014, pp. 918–926.

[31]Huan, X. and Marzouk, Y. M., "Simulation-based optimal Bayesian experimental design for nonlinear systems," *Journal of Computational Physics*, Vol. 232, No. 1, 2013, pp. 288–317.

[32]Villanueva, D. and Smarslok, B. P., "Using Expected Information Gain to Design Aerothermal Model Calibration Experiments," *17th AIAA Non-Deterministic Approaches Conference, Kissimmee, FL, USA*, 2015.

[33]Simpson, T. W., Mauery, T. M., Korte, J. J., and Mistree, F., "Kriging models for global approximation in simulation-based multidisciplinary design optimization," *AIAA journal*, Vol. 39, No. 12, 2001, pp. 2233–2241.

[34]Rasmussen, C. E., "Gaussian processes for machine learning," MIT Press, 2006.

[35]Banach, S., "Sur les opérations dans les ensembles abstraits et leur application aux équations intégrales," *Fund. Math*, Vol. 3, No. 1, 1922, pp. 133–181.

[36]Granas, A. and Dugundji, J., *Fixed point theory*, Springer Science & Business Media, 2013.

[37]Phillips, W. and Snyder, D., "Modern adaptation of Prandtl's classic lifting-line theory," *Journal of Aircraft*, Vol. 37, No. 4, 2000, pp. 662–670.

[38] Jasa, J. P., Hwang, J. T., and Martins, J., "OpenAeroStruct: An open-source tool to perform aerostructural optimization," 2017.

[39] "OpenAeroStruct code," `https://github.com/mdolab/OpenAeroStruct`, Accessed: 2017-01-15.

[40] Gray, J., Moore, K., and Naylor, B., "OpenMDAO: An open source framework for multidisciplinary analysis and optimization," *13th AIAA/ISSMO Multidisciplinary Analysis Optimization Conference*, 2010, p. 9101.